12-1990

Dendrite Tip Radii in Directionally Solidified Pb-8.4-Atmospheric-Percent-Au

Surendra N. Tewari
Cleveland State University, s.tewari@csuohio.edu

Dendrite Tip Radii in Directionally Solidified Pb–8.4at.%Au

S. N. TEWARI

Chemical Engineering Department, Cleveland State University, Cleveland, OH 44135 (U.S.A.)

Abstract

The cell/dendrite tip radii in directionally solidified Pb–8.4at.%Au have been investigated as a function of the growth speed and thermal gradient in the liquid at the tip. Dendrite growth models are not able to predict quantitatively the tip radii and tip compositions separately because of the occurrence of thermosolutal convection during growth. However, the relationship between the destabilizing solutal gradient, the stabilizing thermal gradient and the capillarity at the tip assumed using the "marginal stability" criterion is supported by the experimental data.

1. Introduction

Understanding the development of cellular and dendritic microstructures during solidification is crucial in relating the solidification parameters to the microstructures of cast alloys and their effects on mechanical properties. Mullins and Sekerka [1] derived the following relationship to define the transition from a stable to an unstable solid–liquid interface by performing a linear stability analysis for the steady-state growth of a planar interface:

$$m_l G_c^p[1 + g(w)] - G^p \geqslant T_m \Gamma w^2 \qquad (1)$$

where m_l is the liquidus slope, T_m is the alloy liquidus temperature, Γ is the capillary length, equal to the ratio of the solid–liquid interfacial energy and the volumetric heat of fusion (L_V), and $g(w)$ is a function of the perturbation wave number, w. The thermal gradients at the interface in the solid (G_s) and liquid (G_l) are combined together in the parameter G^p, the effective thermal gradient, which is equal to

$$(K_l G_l + K_s G_s)/(K_s + K_l)$$

where K_s and K_l are the thermal conductivities of the solid and liquid phases. Figure 1 shows schematically G_c^p, the concentration gradient in the liquid, and $(2\pi/w)$, the shortest instability wavelength for a planar solid–liquid interface.

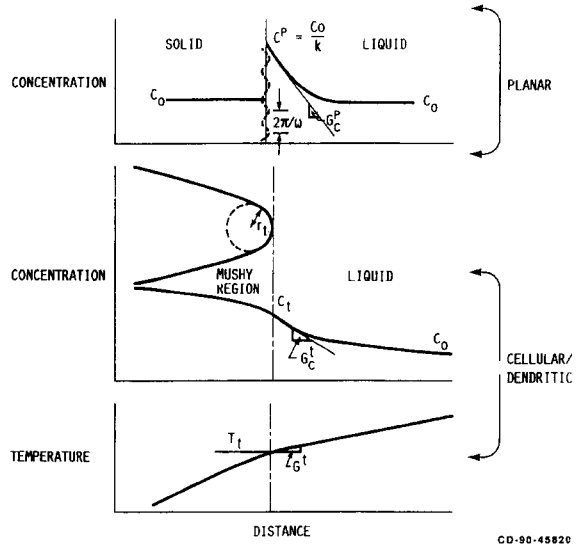

Fig. 1. Schematic representation of "marginal stability". The minimum unstable wavelength for a planar liquid–solid interface $(2\pi/w)$ is assumed to be equal to the cell/dendrite tip radius, r_t. The thermal (G_p) and solutal (G_c^p) gradients in the linear stability analysis for a planar interface [1] are replaced with those at the dendrite tip, G^t and G_c^t.

A similar rigorous stability analysis has not been possible for cellular/dendritic liquid–solid interfaces due to their complex, non-planar shapes. Instead, as shown schematically in Fig. 1, the approach taken in the literature [2–10] has been to use eqn. (1), with an equal sign, as the stability expression for a cellular or dendritic interface, by replacing the solutal and thermal gradients for the planar interface with those at the dendrite tip, G_c^t and G_t. Following the marginal stability criterion suggested by Langer and Muller-Krumbhaar [2], the cell or dendrite tip radius (r_t) is taken to be equal to the shortest instability wavelength for the planar interface, *i.e.*

$$w = 2\pi/r_t$$

It has recently been suggested that the marginal stability criterion is inaccurate as compared with the more rigorous "principle of microscopic solvability" [11, 12]. However, the strength of its physics has been demonstrated amply by its quantitative prediction of the experimentally observed dendrite growth speed and tip radius dependence on undercooling in well-characterized experiments on succinonitrile [4].

This criterion requires the ratio

$$(m_l G_c^t - G^t)/(4\pi^2 \Gamma T_m/r_t^2)$$

to be equal to unity for small solute Peclet numbers, $p = Rr_t/2D_l$, because of the factor $[1 + g(W)]$ in eqn. (1) being approximately equal to unity [1]. Here R is growth speed and D_l is the solute diffusivity in the melt. During free growth of dendrites in a single-component undercooled melt $G_c^t = 0$, and the thermal gradient G^t cannot be measured directly; instead it is calculated by assuming the tip to be a spherical particle solidifying into the undercooled melt [4]. On the other hand, constrained growth of cellular/dendritic microstructures in binary alloys in a positive thermal gradient should allow direct experimental measurement of all three parameters G_c^t, G^t and r_t, for a more critical evaluation of the marginal stability criterion. The effective thermal gradients, given by

$$G^t = [(2K_l G_l + RL_v)/(K_s + K_l)]$$

can be estimated from the experimentally measured G_l and the thermal conductivities of the liquid (K_l) and solid (K_s) phases. Ignoring the much smaller diffusivity of solute into the solid, the solutal gradient in the melt at the tip, G_c^t, can be obtained by the solute flux balance at the tip:

$$G_c^t = -RC_t(1-k)/D_l$$

The composition of liquid in equilibrium with the tip, C_t, is related to the tip temperature T_t, given by

$$T_t = T_m + m_l C_t - 2\Gamma T_m/r_t$$

where T_m is the melting point of the solvent. r_t, T_t and C_t can be measured by techniques reported previously [13–18].

Analytical models for dendrite growth during steady-state directional solidification of binary alloys in a positive thermal gradient have been developed by solving the appropriate thermal and solutal transport equations to obtain an analytical relationship between the solute Peclet number, p, and the concentration gradient at the tip, G_c^t. One further relationship between r_t and G_c^t is required for *independent predictions of the tip radius and tip composition* as a function of alloy composition C_0, growth speed, thermal gradient and physical properties of the alloy. This relationship is obtained by employing an assumption, for example minimum undercooling at the dendrite tip [14, 19], or marginal stability at the dendrite tip [5–10]. The marginal stability criterion generally provides good quantitative agreement with experiments for transparent organic alloys, both for dendrites growing in an undercooled melt [4] and for directional solidification [14]. Kurz and Fisher [5] used an isolated paraboloidal dendrite (Ivantsov approach) as the basis for thermal and solutal transport, and they combined the marginal stability criterion of Langer and Muller-Krumbhaar [2] to predict the dendrite growth behaviour. Trivedi [6] introduced the thermal gradient and capillarity into the Ivantsov approach and used the marginal stability of a spherical solid [20] to predict r_t, T_t and C_t. Laxmanan [7] used the approach of Burden and Hunt of obtaining C_t by combining the divergent solutal field due to curvature and the "average solute concentration ahead of the growth front depending mainly on G_l" [14], and then used the marginal stability approaches of Langer and Muller-Krumbhaar [2] and Trivedi [20] to predict the growth behaviour of dendrites. This approach predicts that at low Peclet number

$$2l_c D_l/Rr_t^2 = A(1-s)$$

where l_c is the capillary length and is equal to $\Gamma/m_l C_0(k-1)$, k being the partition coefficient. The parameter $(1-s)$ is a measure of the gradient of constitutional supercooling.

$$s = D_l G_l k/m_l R C_0 (k-1)$$

Its value is zero for planar liquid–solid interfaces. It increases towards a maximum value of one as the microstructure first becomes cellular and then dendritic. The value of the constant A is equal to $1/2\pi^2$ for the assumption of "marginal stability" used by Langer and Muller-Krumbhaar [2] and is equal to $1/28$ for the "marginal stability" approach of Trivedi [21]. All of these models assume a steady-state growth involving purely diffusive thermal and solutal transport and do not distinguish between the cells and dendrites.

The literature contains many reports of careful examinations of the dendrite tip morphology in directionally solidified, optically transparent succinonitrile and pivalic acid alloys [15, 16, 21, 22] and metallic alloys [13, 14, 17, 18, 23, 24]. However, there have been few studies in which *simultaneous* measurements of C_t or T_t and r_t have been reported for cellular and dendritic microstructures. There is one datum for the alloy Fe–8%Ni alloy [24]. Miyata *et al.* [17] have reported measurements on Al–4.1wt.%Cu. Esaka and Kurz [16] have reported measurements on a succinonitrile–1.3wt.%acetone alloy. Sharp and Hellawell [13] studied Al–2%Cu; however, it is not possible to extract C_t or r_t from this paper.

The main purpose of this investigation was to examine the growth rate and thermal gradient dependence of the cellular/dendritic tip radii in binary Pb–8.4at.%Au alloy directionally solidified with a positive thermal gradient, and to compare the experimental behaviour with predictions from theoretical models. Another objective was to determine if the ratio

$$(m_l G_c^t - G^t)/(4\pi^2 \Gamma T_m / r_t^2)$$

is equal to unity for constrained growth of cellular/dendritic microstructures, as is assumed by the marginal stability criterion.

The Pb–8.4at.%Au alloy was originally selected to minimize gravity-driven convection, because increasing the solute content of the melt produces an increased melt density. However, as reported earlier [23, 25], the longitudinal sections of many of these specimens showed non-uniform cell lengths across the specimen diameter. Until recently it has not been understood whether this "steepling" effect is due to gravity-driven settling of the solute-rich higher density liquid as has been suggested [25, 26], or to natural convection resulting from a transverse thermal gradient in the melt. The effect is in fact caused by gravity as has been demonstrated recently by its absence in an Al–26.5wt.%Cu specimen grown aboard the space shuttle [27]. Steepling results in considerable distortion of the solid–liquid interface near the tips.

This paper shows that the predictions from the dendrite growth models do not exhibit quantitative agreement with the experimentally observed tip radii because they do not include convection in their analysis. It is interesting, however, that although the tip radii and the tip composition are affected by convection, their interrelationship for Pb–Au alloys still follows the marginal stability criterion, for both the cellular and the dendritic microstructures. Examination of the available data on succinonitrile–1.3wt.%acetone [16] and Al–4.1wt.%Cu [17] shows that the value of the ratio

$$(m_l G_c^t - G^t)/(4\pi^2 \Gamma T_m / r_t^2)$$

is higher for dendrites than for cells.

2. Experimental details

The partially directionally solidified and quenched Pb–8.4at.%Au specimens used in this study were prepared by Mason *et al.* [28] in work previously reported. Figure 2 shows longitudinal sections through the quenched liquid–solid interface for typical specimens examined in this study. These micrographs represent the entire width of the specimen. Figure 2(a) shows a cellular microstructure with a small cell length (distance from the base of primary dendrite at the eutectic isotherm to its tip). In this figure the eutectic isotherm is easily identified by the presence of intercellular eutectic at the base of the cells. As mentioned earlier, the macro liquid–solid interface near the quenched cell/dendrite tips is distorted, *i.e.* the cell lengths are not uniform across the specimen cross-section. The extent of this distortion was observed to increase with increasing G_l/R [23]. Specimens solidified at a growth speed of 10 μm s^{-1} or higher did not show such distortion (Fig. 2(b)). Figure 2(b) shows a dendritic microstructure with a much larger cell length.

The cell/dendrite tip radii were measured by serial sectioning parallel to the alloy growth direction in a manner reported earlier [18]. Longitudinal microstructures for several cells/dendrites were recorded during successive polishing. When these sections made from one side of the dendrite to the other side were superimposed, the actual longitudinal mid-section through the dendrite was identified as the one protruding the most into the quenched melt ahead. About 10 to 15 sections were usually required to ensure that the morphology across the tip corresponding to the actual mid-section of the primary dendrite was obtained. The micrographs in Fig. 3 show five typical sections through a cell in a sample grown at a speed of 0.6 μm s^{-1} ($G_l = 203$ K cm^{-1}). Figure 4 shows the superimposition of several such sections through the cell/dendrite tips for four typical growth conditions. The G_l and R

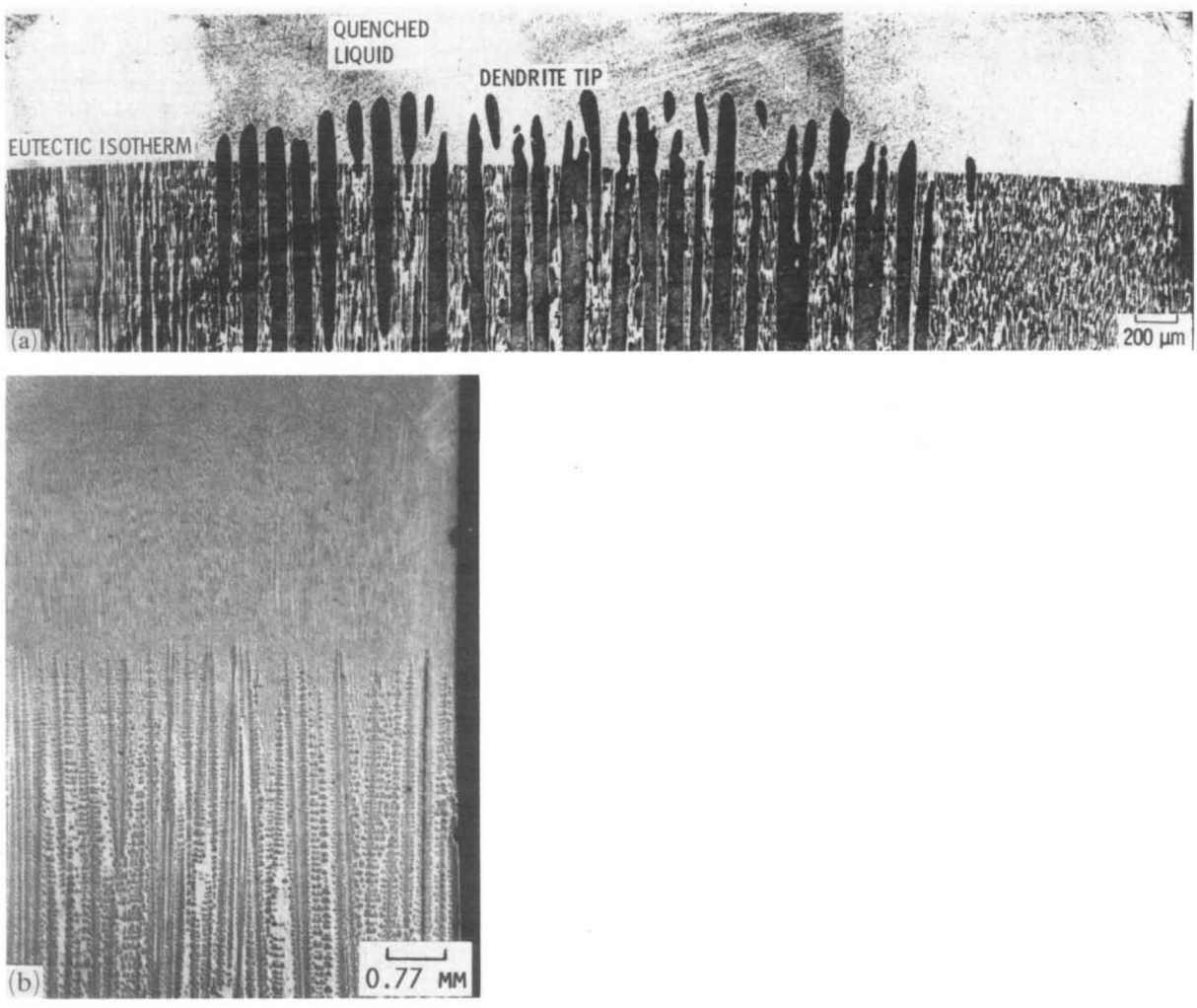

Fig. 2. Longitudinal sections (parallel to the growth direction) through the quenched liquid–solid interface in directionally solidified Pb–8.4 at.% Au: (a) cellular, $R = 0.4\ \mu m\ s^{-1}$, $G_l = 205\ K\ cm^{-1}$; (b) dendritic, $R = 10\ \mu m\ s^{-1}$, $G_l = 281\ K\ cm^{-1}$.

values are given in the caption. As shown in this figure, the superimposition of parallel serial sections (broken curves) were used to locate the actual mid-section (solid curve) near the dendrite tip. As shown in Figs. 4(a) and 4(b), for most of the samples the eutectic isotherm (Fig. 2(a)) provided the common reference to locate the base from the various sections of the dendrite while superimposing them on top of each other. The section which showed the maximum protrusion from the eutectic isotherm was identified as the mid dendrite section (Figs. 4(a) and 4(b)). However, for specimens with relatively large cell lengths (Fig. 2(b)), or for those where the dendrites were not perfectly aligned perpendicular to the eutectic isotherm, this technique could not be used. In such a situation some features near the dendrite tip region (*e.g.* several side branches) were used as the common reference to superimpose the various sections of the dendrite on top of each other (Figs. 4(c) and 4(d)). Specimens 13-52 and CK-125 (Table 1) had such microstructures, so their tip radii are likely to be more subjective and not as accurate as those obtained in the manner described earlier.

A parabolic fit (curves marked P in Fig. 4) to the dendrite mid-section was used to obtain the tip radius. These parabolas show a deviation from the actual tip profile (solid line) as one moves away from the tip towards the base of the dendrites. As the microstructure changes from cellular to dendritic, the distance from the tip along the length of the dendrite at which this deviation occurs increases. For example, the ratio of this distance to the measured tip radius is only about 2.5 for the specimen with the cellular microstruc-

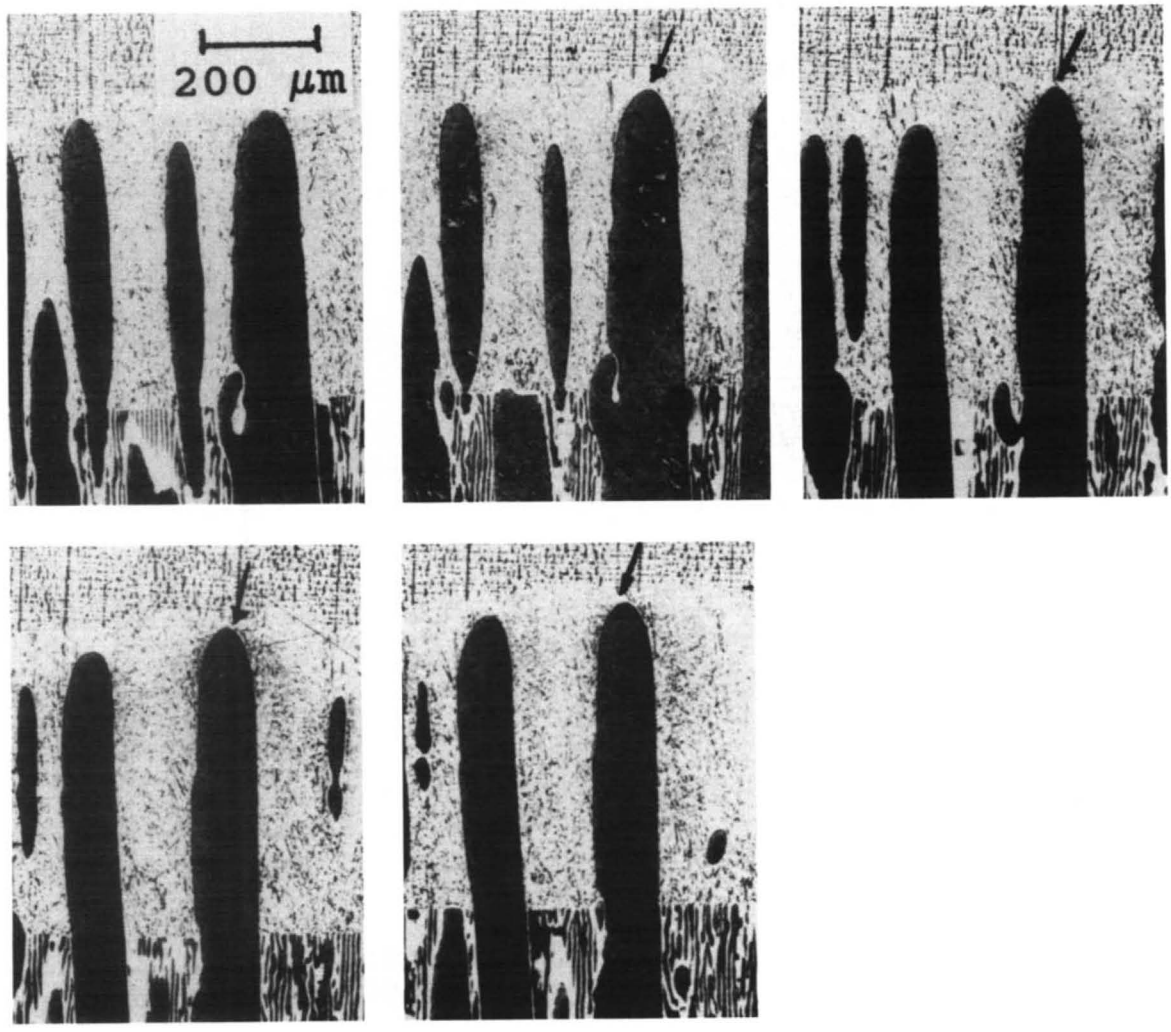

Fig. 3. Some of the typical sections through a cell which were used to locate the mid-dendrite tip shape and to measure the tip radius. $R = 0.6\ \mu m\ s^{-1}$, $G_l = 203\ K\ cm^{-1}$.

ture (Fig. 4(a), $G_l/R = 5.62 \times 10^6$ K s cm^{-2}), whereas it is 18 and 10 for the dendritic microstructures of Figs. 4(c) and 4(d) ($G_l/R = 3.52 \times 10^6$ and 2.2×10^6 K s cm^{-2} respectively). The dendritic features can therefore certainly be assumed to be paraboloidal at the tip. The cellular microstructures, on the other hand, cannot be depicted accurately by a paraboloidal tip. However, in order to maintain consistency in this analysis the tip radii reported here have all been obtained by the parabolic fit.

The tip compositions of quenched liquid at the dendrite tips measured using electron microprobe analysis and reported in ref. 23 will be used in this paper. These were measured only for the cells/dendrites having the largest cell/dendrite lengths. The scatter in the values reported in ref. 23 is from measurements on several such cells/dendrites in a sample.

3. Results and discussion

In this section we will first examine the measured tip radii and compare them with predictions from cell/dendrite growth models. We will then use the tip composition data [23] together with the tip radii values to examine the validity of marginal stability, *i.e.* to see if the ratio

$$(m_l G_c^t - G^t)/(4\pi^2 \Gamma T_m / r_t^2)$$

is unity for Pb–8.4at.%Au. Finally we will examine this ratio for Al–Cu [17] and succinonitrile–acetone [16] alloys. The thermophysical

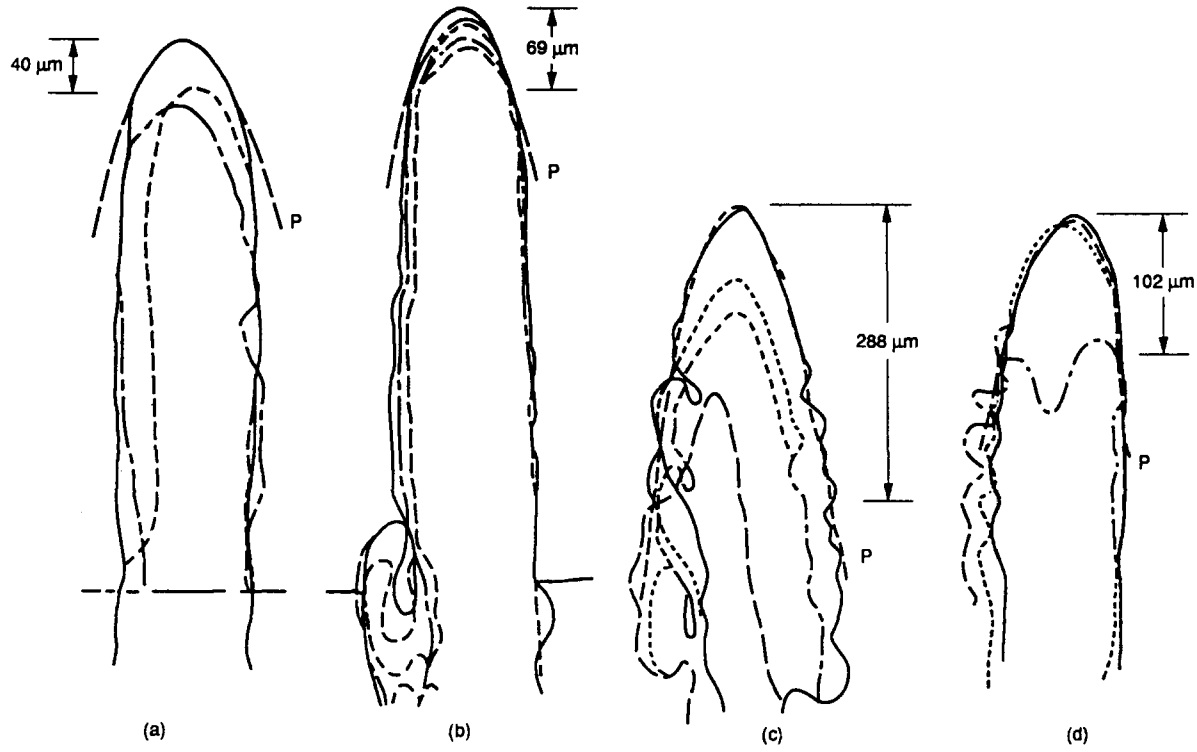

Fig. 4. Typical cell/dendrite tip morphology in directionally solidified Pb–8.4 at.% Au. Curves denoted by 'P' are the parabolas which were fitted to the tips to obtain the tip radii: (a) cellular microstructure, $G_l = 225$ K cm^{-1}, $R = 0.4$ μm s^{-1}; (b) mixed (cellular/dendritic) microstructure, $G_l = 203$ K cm^{-1}, $R = 0.6$ μm s^{-1}; (c) dendritic microstructure, $G_l = 140$ K cm^{-1}, $R = 0.4$ μm s^{-1}; (d) dendritic microstructure, $G_l = 220$ K cm^{-1}, $R = 1$ μm s^{-1}.

TABLE 1 Thermophysical properties of Pb–8.4at.%Au used in the present analysis

Liquidus temperature (T_L)	541.7 K
Eutectic temperature (T_e)	488.0 K
Eutectic composition (C_e)	15.97 at.% Au
Alloy composition (C_0)	8.38 at.% Au
Solute diffusivity in melt (D_L)	9.8×10^{-6} cm^2 s^{-1}
Liquid–solid surface energy (ν)	46×10^{-7} J cm^{-2}
Solute partition coefficient (k)	≈ 0.006 at.% (at.%)$^{-1}$
Entropy of fusion (ΔS)	243.6/600.6 J cm^{-3} K
Slope of liquidus (m_L)	7.07 K (at.%)$^{-1}$

properties of Pb–8.4at.%Au used in these calculations are listed in Table 1. For Al–Cu and succinonitrile–acetone the thermophysical properties compiled in ref. 29 have been used.

3.1. Cell/dendrite tip radius

Table 2 lists the tip radii and corresponding cell lengths for the Pb–8.4at.%Au samples grown using varying thermal gradients and growth velocities. In the same specimen the longer dendrites/cells located in the central portion of the sample generally showed larger tip radii than those with the smaller lengths (Table 2). Only the average tip radii for the cells/dendrites located near the centre of the specimen cross-section (those for the longest cell/dendrite lengths) will be used in the following analysis. The tip radii data for specimens 13–52 and CK-125 (Table 2) will be excluded because of the reasons mentioned earlier. The convection effects will be neglected.

The experimentally observed growth velocity and thermal gradient dependences of the dendrite tip radii are represented in Fig. 5, where $\sigma_c = 2l_c D_l / R r_t^2$ is plotted as a function of G_l/R. The open symbols correspond to the cellular microstructure and the closed symbols represent the dendritic microstructure. The square represents a mixed (cellular/dendritic) microstructure. The two arrows on the left-hand side of this figure show the σ_c values predicted from the two marginal stability approaches described earlier of Langer and Muller-Krumbhaar ($A = 1/2\pi^2$) and Trivedi ($A = 1/28$). Because of the very low value of k (0.006) and since $s = 0$ for Pb–Au, the value of $2l_c D_l / R r_t^2$ is predicted to be equal to A [7]. Owing to the very large scatter in the data in Fig. 5, it is not possible to draw definite conclusions

TABLE 2 Dendrite tip radii in directionally solidified Pb–8.4 at.% Au alloy. (MS represents "marginal stability")

Specimen	*Growth velocity* ($\mu m\ s^{-1}$)	*Gradient* ($K\ cm^{-1}$)	*Cell length* (μm)	*Tip radius* (μm)		
				Experiment	*Theory*	
					Ivantsov + MS	*Burden and Hunt + MS*
13-27	0.4	140	1192	16.0	20.0	15.6
			1181	16.0		
			923	13.3		
			743	10.4		
			603	10.4		
CK-130	2.0	409	1175	4.9	7.9	7.0
			1167	7.5		
			1134	6.7		
			1105	4.9		
			1100	7.5		
			1114	7.6		
13-44	1.0	84	4121	6.5	10.2	9.9
			4051	6.5		
			4018	8.5		
			3820	6.9		
			3750	9.4		
13-23	0.4	225	389	15.9	26.0	15.6
			364	10.4		
			318	13.4		
13-33	0.4	35	9100	17.2	16.5	15.6
13-40	1.0	128	3450	8.3	10.5	9.9
13-47	1.0	220	1219	10.6	11.2	9.9
			1219	10.6		
			1189	9.9		
			1185	10.3		
			1130	10.3		
			933	7.6		
13-105	0.6	203	318	10.3	17.2	12.7
			352	13.7		
			236	8.5		
			246	12.2		
			499	10.7		
			471	9.8		
			508	11.9		
			504	12.1		
			524	13.2		
13-52	10.0	281		6.3	3.1	3.1
				6.5		
CK-125	20.1	361	1440	3.3	2.1	2.2
				3.3		
				2.9		
				2.9		

about the suitability of either of the two approaches. The average of the experimental σ_c values is 0.04, a value in between 1/28 and $1/2\pi^2$.

Theoretical predictions of cell/dendrite tip radii from two typical models are also listed in Table 2 for a direct comparison with the experimentally observed radii. In order to predict the tip radius, the first model combines the marginal stability criterion with the transport relationships of Ivantsov [20], and the second model combines it with the transport relationships of Burden and Hunt [7]. An examination of this table shows that the experimental values are in reasonable agreement with the theoretical predictions. However, the scatter in the data, caused by convection, does not allow us to distinguish between the two models. Accurate measurements of r_t and C_t in binary metallic alloys are possible only in the low growth rate and high thermal gradient regime. Unfortunately, this is the growth regime in which the "steepling" due to convection is maximized [23, 27] and affects the tip radii and tip compositions the most. In solutally stabilizing alloy compositions, such as Al–Cu and Pb–Au, it has not been possible to avoid this problem by selecting

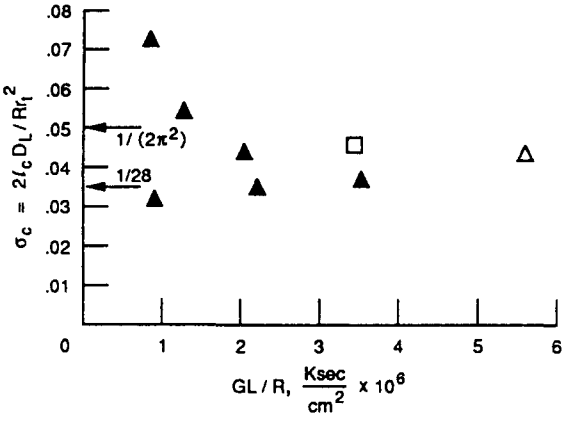

Fig. 5. Dependence of $\sigma_c = 2l_cD_l/Rr_t^2$ on G_l/R for Pb–8.4at.%Au. Open triangles are for cells, closed triangles are for dendrites and squares are for mixed microstructures.

either low solute contents, where the mushy zone will be nearly impermeable to any fluid flow, or by reducing the crucible diameter. Partial directional solidification and quenching experiments, especially near the cell to dendrite transition, carried out in the low gravity environment of space will be highly desirable for a critical evaluation of dendrite growth models.

3.2. Marginal stability

3.2.1. Dendrite tip radius

As discussed above the distortions caused by convection do not allow quantitative predictions of experimentally observed tip radii in Pb–Au specimens using dendrite growth models. This is because only diffusive solutal and thermal transport are incorporated in the models. However, independent measurements of tip radii and tip composition carried out in this study should still allow us to examine the basic physics behind the marginal stability criterion. This criterion is based on the assumption that three effects determine interfacial stability during directional solidification of a binary alloy in a positive thermal gradient: the destabilizing influence of the solutal gradient in the melt ahead of the interface caused by the solute rejected during solidification, the stabilizing influence of the applied positive thermal gradient in the melt, and the stabilizing influence of the liquid–solid surface energy.

According to this criterion the value of $(m_lG_c^t - G^t)/(4\pi^2\Gamma T_m/r_t^2)$ should be equal to unity. Figure 6 plots r_t^{-2} *vs.* $(m_lG_c^t - G^t)$. The tip composition data are taken from ref. 23, and tip radii data from Table 2. The scatter shown on the ordinate and the abscissa denote the experimentally observed variation in tip composition and tip radii. Full symbols are for dendrites and the open symbols are for cells. The line drawn corresponds to a value of unity for $(m_lG_c^t - G^t)/(4\pi^2\Gamma T_m/r_t^2)$. The data show an agreement with the behaviour expected from the marginal stability criterion.

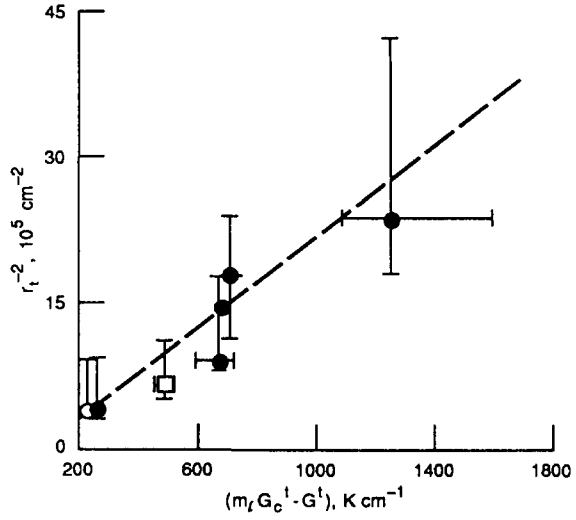

Fig. 6. Plot of r_t^{-2} *vs.* $(m_lG_c^t - G^t)$ for cell/dendrite tip during directional solidification of Pb–8.4at.%Au. The cellular, dendritic and mixed microstructures are indicated by filled symbols, open symbols and a square respectively.

TABLE 3 The experimentally observed ratios $(m_lG_c^t - G^t)/(4\pi^2\Gamma T_m/r_t^2)$ (column (b)) and the corresponding values of $[1 - (G^t/m_lG_c^t)]$ (column (a)), a parameter denoting the gradient of constitutional supercooling at the tip. The cellular, dendritic and mixed microstructures are denoted by c, d and m in parentheses

Pb–Au		*Succinonitrile–acetone [16]*		*Al–Cu [17]*	
(a)	*(b)*	*(a)*	*(b)*	*(a)*	*(b)*
0.584	0.996(c)	0.042	0.256(c)	0.32	0.375(c)
0.743	1.54(d)	0.32	1.66(d)	0.57	0.466(c)
0.785	1.47(m)	0.48	1.93(d)	0.73	0.793(c)
0.822	1.63(d)	0.69	2.25(d)	0.77	2.11(c)
0.822	1.19(d)	0.68	1.2(d)	0.79	3.5(d)
0.928	0.83(d)	0.81	1.48(d)	0.86	4.84(d)
0.89	1.06(d)	0.94	1.57(d)	0.89	4.87(d)
		0.87	1.92(d)	0.94	4.70(d)
				0.96	4.08(d)
				0.98	4.70(d)

Let us now examine the experimentally observed values of the ratio $(m_lG_c^t - G^t)/(4\pi^2\Gamma T_m/r_t^2)$ shown in Table 3. Only the average experimental data (without their scatter) are included in this table. For each experiment, the values of $[1 - (G^t/m_lG_c^t)]$, a parameter denoting the gradient

of constitutional supercooling at the tip, and the type of microstructures ("c", "d" and "m" for the cellular, dendritic and mixed morphologies) are also listed in Table 3. These data can be better visualized in Fig. 7, where the individual experiments are indicated by their $[1-(G^t/m_l G_c^t)]$ values on the ordinate, and the corresponding values of $(m_l G_c^t - G^t)/(4\pi^2 \Gamma T_m/r_t^2)$, from experimental measurements, are plotted on the abscissa. The filled symbols in this figure are for dendritic microstructures which are obtained at higher gradients of constitutional supercooling and the open symbols are for cellular microstructures obtained at lower gradients of constitutional supercooling. The square corresponds to the sample with the mixed (containing both the cells and dendrites) microstructure. The average $(m_l G_c^t - G^t)/(4\pi^2 \Gamma T_m/r_t^2)$ values observed for the cellular and dendritic microstructures of the Pb–Au alloy is 1.24. This is close to the expected value of unity.

The experimentally observed $(m_l G_c^t - G^t)/(4\pi^2 \Gamma T_m/r_t^2)$ ratios for succinonitrile–acetone [16] and aluminium–copper [17] listed in Table 3 are plotted in Figs. 7(b) and 7(c). For succinonitrile–acetone, experimentally measured T_t values are used to determine G_c^t. For Al–Cu experimentally observed C_t values are used to obtain G_c^t. The effective thermal gradients, G^t, are estimated from the experimentally reported G_l and the thermal conductivities of the liquid (K_l) and solid (K_s) phases. The average value of $(m_l G_c^t - G^t)/(4\pi^2 \Gamma T_m/r_t^2)$ for succinonitrile–acetone dendrites is 1.8, which is within a factor of two of the expected value of unity. This much scatter may be attributed to the uncertainties in the experimental data and the physical properties used in this analysis.

For the dendritic microstructures of Al–Cu alloy this value is significantly larger, about 4.6. One may, however, still argue that this is because of uncertainties in the physical parameters. For example, a smaller value of D_l, say 3×10^{-5} [13], instead of 5×10^{-5} [29] as was used in this study, will make $(m_l G_c^t - G^t)/(4\pi^2 \Gamma T_m/r_t^2)$ equal to 2.8 for Al–Cu.

3.2.2. *Cellular morphology*

There have been several theoretical investigations [30–34] to describe the growth of the cellular array. The numerical analyses of Unger and Brown [30] and McFadden and Coriell [31] were aimed at the development of the cells during the initial breakdown of a planar liquid–solid interface. The numerical work of Hunt and McCartney [32] attempted to describe the steady-state growth of the cellular array. Pelce and Pumir [33] have used the analogy between Saffman–Taylor fingers [34] and the cellular array to develop an analytical solution. It has been shown by Hunt and McCartney [32] that their marginal stability analysis does not predict the cell spacings in Al–Cu alloys. Meaningful comparisons with

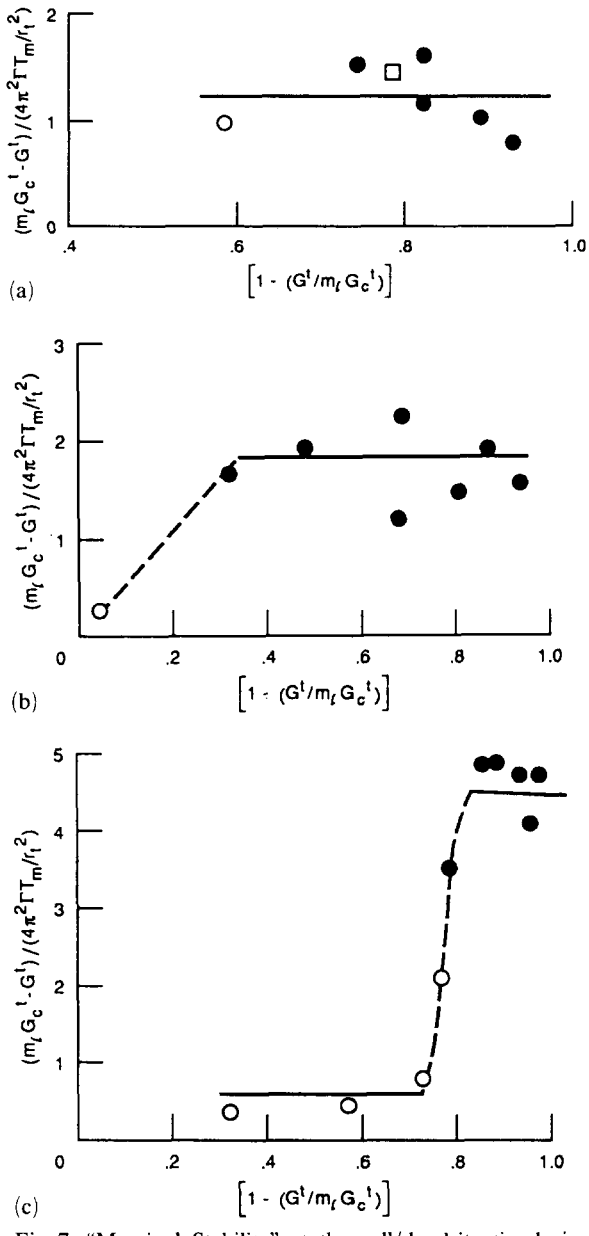

Fig. 7. "Marginal Stability" at the cell/dendrite tip during directional solidification of binary alloys. The cellular and dendritic microstructures are indicated by filled and open symbols: (a) Pb–8.4at.%Au, (b) succinonitrile–1.3wt.%-acetone [16], (c) Al–4.1wt.%Cu [17].

theoretical models are, however, not possible for the cellular morphology because, unlike the dendritic microstructures, the r_t and G_c data for cells are very limited (Figs. 6 and 7). However, it is interesting to note that unlike Pb–Au (Figs. 6 and 7(a)) in which cells and dendrites possess the same values for the ratio $(m_l G_c^t - G^t)/(4\pi^2 \Gamma T_m / r_t^2)$, both Al–Cu and succinonitrile–acetone (Figs. 7(b) and 7(c)) show it to be much higher for the dendrites as compared with the cells. The reason for this behaviour is not clear; it may be related to the partition coefficients.

The composition gradient at the cell/dendrite tip (G_c^t) is made up of two contributions: one from the divergent solute field due to tip curvature $(\hat{G}_c)$ and one from the interdendritic solute diffusion from behind the tip $(\bar{G}_c)$ [14, 19]. Their ratio is given as [14, 19]

$$(\hat{G}_c)/(\bar{G}_c) = (1-s)k/[1-p(1-k)]$$

The magnitude of their ratio is expected to increase with increasing degree of constitutional supercooling $(1-s)$. The curvature contribution $\hat{G}_c$ will be almost zero for Pb–Au alloys because of their low partition coefficient $(k = 0.006)$; G_c^t is mostly made up of $\bar{G}_c$ for cells and dendrites. Cells and dendrites are therefore expected to show similar behaviour. In contrast, for Al–Cu $(k = 0.14)$ and succinonitrile–acetone $(k = 0.1)$ the curvature contribution increases with increasing degree of constitutional supercooling, as the microstructure changes from cellular to dendritic. The cells and dendrites therefore show different behaviours. However, more experimental data for three-dimensional cellular arrays are critically needed for meaningful analysis of the theoretical models and for evaluating the applicability of marginal stability.

4. Concluding remarks

Directional solidification of Pb–8.4at.%Au specimens in growth conditions which should have been thermally and solutally stable is nevertheless affected by gravity-driven convection. This influences the solutal profile in the melt ahead of the cellular/dendritic interface and the morphology of the dendrite tips. The tip radii and tip compositions are therefore not individually predicted satisfactorily by dendrite growth theories. However, the relationship between the destabilizing solutal gradient in the melt, the stabilizing thermal gradient and the stabilizing capillarity effects at the liquid–solid interface, assumed by the marginal stability criterion in determining the cell/dendrite tip radii, appears to be supported by data on Pb–Au alloys. Data from the literature on Al–Cu and succinonitrile–acetone dendrites also support marginal stability. However, the ratio $(m_l G_c^t - G^t)/(4\pi^2 \Gamma T_m / r_t^2)$ (which was the same for both the cells and the dendrites in Pb–Au) is higher for dendrites than for cells for both Al–Cu and succinonitrile–acetone. This may be because of the differences in solute partition coefficients. However, there are very few data available on simultaneous measurements of tip radii and tip temperature or tip composition in metallic alloys, especially in the cellular growth regime. Based on the experimental evidence to date it appears that tip morphology and tip composition data in metallic alloys, required for quantitative comparison with cell/dendrite growth theories, can only be obtained from directional solidification and quenching experiments carried out in the microgravity environment of space.

Acknowledgments

This work was funded by the "NASA-Microgravity Science and Applications Program" under Grant NCC-395. Research was carried out in the Microgravity Materials Science Laboratory at NASA Lewis Research Center, Cleveland, Ohio. Dr. J. T. Mason and Professor R. Trivedi very kindly made the directionally solidified Pb–Au alloy specimens available for this study. Appreciation is expressed to Professor R. Trivedi and Dr. V. Laxmanan for their helpful comments, and to David Lee for his help in metallography.

References

1 W. W. Mullins and R. F. Sekerka, *J. Appl. Phys., 34* (1963) 444–451.
2 J. S. Langer and H. Muller-Krumbhaar, *Acta Metall., 26* (1978) 1681–1687.
3 G. P. Ivantsov, *Dokl. Akad. Nauk. SSSR, 58* (1947) 567. (Engl. Transl.: *NASA Tech. Memo 77889.*)
4 S. C. Huang and M. E. Glicksman, *Acta Metall., 29* (1981) 701–715.
5 W. Kurz and D. J. Fisher, *Acta Metall., 29* (1981) 11–20.
6 R. Trivedi, *J. Cryst. Growth, 49* (1980) 219–232.
7 V. Laxmanan, *J. Crystal Growth, 83* (1987) 573–590.
8 R. Trivedi, J. Lipton and W. Kurz, *Acta Metall., 35* (1987) 965.
9 J. Lipton, M. E. Glicksman and W. Kurz, *Mater. Sci. Eng., 65* (1) (1984) 57–64.

10 W. Kurz and D. J. Fisher, *Fundamentals of Solidification*, Trans Tech, Aedermannsdorf, 1986, p. 77.
11 D. A. Kessler and H. Levine, *Acta Metall., 36* (1988) 2693–2706.
12 J. S. Langer, *Science, 243* (1989) 1150–1156.
13 R. M. Sharp and A. Hellawell, *J. Cryst. Growth, 6* (1970) 253–260.
14 M. H. Burden and J. D. Hunt, *J. Cryst. Growth., 22* (1974) 909–916.
15 K. Somboonsuk, J. T. Mason and R. Trivedi, *Metall. Trans. A, 15* (1984) 967–975.
16 H. Esaka and W. Kurz, *J. Cryst. Growth, 72* (1985) 578–584.
17 Y. Miyata, T. Suzuki and J. I. Uno, *Metall. Trans. A, 16* (1985) 1799–1805.
18 S. N. Tewari, *Metall. Trans. A, 17* (1986) 2279–2290.
19 V. Laxmanan, *Acta Metall., 33* (1985) 1023–1049.
20 R. Trivedi, *Acta Metall., 18* (1979) 287.
21 R. Trivedi, *Metall. Trans. A, 15* (1987) 977–982.
22 M. A. Eshelman, V. Seetharaman and R. Trivedi, *Acta Metall., 36* (1988) 1165–1174.
23 S. N. Tewari, *Metall. Trans. A, 19* (1988) 1351–1363.
24 I. Jin and G. R. Purdy, *J. Cryst. Growth, 23* (1974) 37–44.
25 J. D. Verhoeven, J. T. Mason and R. Trivedi, *Metall Trans. A, 17* (1986) 991–1000.
26 M. H. Burden, D. J. Hebditch and J. D. Hunt, *J. Cryst. Growth, 20* (1978) 121–124.
27 M. D. Dupouy, D. Camel and J. J. Favier, *Acta Metall., 37* (1989) 1143–1157.
28 J. T. Mason, J. D. Verhoeven and R. Trivedi, *Metall. Trans. A, 15* (1980) 1665–1676.
29 S. DeCheveigne, C. Guthmann, P. Kurowski, E. Vicente and H. Billoni, *J. Cryst. Growth, 92* (1988) 616–628.
30 L. H. Unger and R. A. Brown, *Phys. Rev. B, 29* (1984) 1367; *30* (1984) 3993; *31* (1984) 5931.
31 G. B. McFadden and S. R. Coriell, *Physica D, 12* (1984) 253.
32 J. D. Hunt and D. C. McCartney, *J. Cryst. Growth, 35* (1987) 89–99.
33 P. Pelce and A. Pumir, *J. Cryst. Growth, 73* (1985) 337.
34 P. G. Saffman and G. I. Taylor, *Proc. R. Soc. London Ser, A, 245* (1958) 312.